EUROPEAN ORGANIZATION FOR NUCLEAR RESEARCH (CERN)

Measurement of the Λ_c^+ to D^0 production ratio in peripheral PbPb collisions at $\sqrt{s_{NN}} = 5.02$ TeV

LHCb collaboration[†]

Abstract

We report on a measurement of the Λ_c^+ to D^0 production ratio in PbPb collisions at $\sqrt{s_{NN}} = 5.02$ TeV with the LHCb detector in the forward rapidity region $2 < y < 4.5$. The Λ_c^+ (D^0) hadrons are reconstructed via the decay channel $\Lambda_c^+ \to pK^+\pi^-$ ($D^0 \to K^-\pi^+$) for $2 < p_T < 8$ GeV/c and in the centrality range of about 65–90%. The results show no significant dependence on p_T, y or the mean number of participating nucleons. They are also consistent with similar measurements obtained by the LHCb collaboration in pPb and Pbp collisions at $\sqrt{s_{NN}} = 5.02$ TeV. The data agree well with predictions from PYTHIA in pp collisions at $\sqrt{s} = 5$ TeV but are in tension with predictions of the Statistical Hadronization model.

Submitted to JHEP

[†]Authors are listed at the end of this paper.

1 Introduction

Historically, heavy flavor (HF) hadrons have been extensively used to study the deconfined state of hadronic matter, the Quark-Gluon Plasma (QGP) [1–3], in particular at the LHC and RHIC [4, 5]. Because of their high masses exceeding the QCD energy scale, HF are produced at an early stage of the collision and experience the full evolution of the colliding medium. Medium-induced energy loss has been studied by measuring the so-called nuclear modification factor (R_{AA}), defined as the ratio of the production yield in nucleus-nucleus (AA) collisions to the one in pp collisions scaled by the number of binary nucleon-nucleon collisions. The measurements of the production cross-section, together with studies of the elliptic flow, indicate a strong interaction between HF and the deconfined medium.

In addition, HF hadrons provide a good laboratory to study hadronization. In particular, baryon-to-meson production ratios are of great interest as they are only sensitive to hadronization. Many measurements have been carried on in e^+e^- [6–8] and pp collisions [9–11] to measure fragmentation functions of heavy hadrons, the latter being extensively used to describe hadron production at high transverse momentum (p_T). However, recent measurements of the Λ_c^+ to D^0 production ratio[1] ($R_{\Lambda_c^+/D^0}$) challenge understanding of hadronization. At the LHC, ALICE has measured the charmed baryon-to-meson ratio at mid-rapidity in pp, pPb and PbPb collisions at $\sqrt{s} = 7$ TeV and $\sqrt{s_{NN}} = 5.02$ TeV, respectively [12–14]. An enhancement compared to predictions of the pp event generator PYTHIA 8 [15] without the color reconnection (CR) mechanism is found both in pp and pPb data at low p_T. The PbPb result, obtained for $p_T > 6$ GeV/c, is compatible with various theory models [16] predicting a large enhancement of the ratio compared to pp and pPb collisions. Similarly, CMS [17] has performed the same measurement at mid-rapidity in pp and PbPb collisions at $\sqrt{s_{NN}} = 5.02$ TeV, for $p_T > 5$ GeV/c. In this case the data are well described by PYTHIA 8 only when the CR mechanism is allowed. At the RHIC collider, the STAR collaboration has also measured $R_{\Lambda_c^+/D^0}$ at mid-rapidity in Au-Au collisions at $\sqrt{s_{NN}} = 200$ GeV [18]. An enhanced baryon-to-meson ratio is found at low p_T compared to scaled pp collisions. It is worth mentioning that both ALICE and STAR measurements in AA collisions can be described by a coalescence hadronization mechanism [16, 19] in which quarks can (re)combine with close-by partons in the QGP to form hadrons. Other predictions based on the Statistical Hadronization Model (SHM) [20, 21] have successfully described the charmed baryon-to-meson ratio measured at RHIC and LHC.

As mentioned, ALICE, CMS and STAR measure a $R_{\Lambda_c^+/D^0}$ in heavy-ion collisions at mid-rapidity, with raising trend from low to intermediate transverse momentum. On the other hand, LHCb has measured a ratio with no p_T dependence in pPb collisions at $\sqrt{s_{NN}} = 5.02$ TeV in the rapidity range $2 < y < 4.5$ [22]. These results correspond to smaller $R_{\Lambda_c^+/D^0}$ values compared to measurements by other experiments, and are fully compatible with predictions from cold nuclear matter effects [23, 24]. The LHCb results are yet to be compared with a coalescence based model. These differences between mid and forward rapidity results indicate a strong rapidity dependence of this ratio, and motivate further studies to better improve the model predictions in different phase-space regions.

This paper presents the first measurement of $R_{\Lambda_c^+/D^0}$ production cross-section ratio in the forward rapidity region in peripheral PbPb collisions at $\sqrt{s_{NN}} = 5.02$ TeV by the LHCb

---

[1]If not stated otherwise, charge conjugation is assumed throughout the article.

collaboration. The paper is organized as follows. Section 2 briefly presents the detector and the data sample. Section 3 describes the analysis steps, from the signal extraction to the estimation of efficiency corrections. The sources of systematic uncertainties are given in Sec. 4. The results are presented and compared to theory predictions in Sec. 5, and conclusions are summarized in Sec. 6.

2   Detector and data selection

The LHCb detector [25, 26] is a single-arm forward spectrometer covering the pseudorapidity range $2 < \eta < 5$, designed for the study of particles containing b or c quarks. The detector includes a high-precision tracking system consisting of a silicon-strip vertex detector (VELO) surrounding the interaction region [27], a large-area silicon-strip detector located upstream of a dipole magnet (UT) with a bending power of about $4\,\mathrm{Tm}$, and three stations of silicon-strip detectors and straw drift tubes [28] placed downstream of the magnet. The tracking system provides a measurement of the momentum, p, of charged particles with a relative uncertainty that varies from 0.5% at low momentum to 1.0% at $200\,\mathrm{GeV}/c$. The minimum distance of a track to a primary collision vertex (PV), the impact parameter (IP), is measured with a resolution of $(15 + 29/p_\mathrm{T})\,\mu\mathrm{m}$, with p_T in GeV/c. Different types of charged hadrons are distinguished using information from two ring-imaging Cherenkov detectors [29]. Photons, electrons and hadrons are identified by a calorimeter system consisting of scintillating-pad and preshower detectors (SPD), an electromagnetic (ECAL) and a hadronic (HCAL) calorimeter. Muons are identified by a system composed of alternating layers of iron and multiwire proportional chambers [30]. The online event selection is performed by a trigger [31], which consists of a hardware stage, based on information from the calorimeter and muon systems, followed by a software stage, which applies a full event reconstruction.

The PbPb collision data at $\sqrt{s_\mathrm{NN}} = 5.02$ TeV were recorded in 2018 and correspond to an integrated luminosity of about $210\,\mu\mathrm{b}^{-1}$. Offline quality selections are applied on a run-by-run basis, based on the trend of trigger counts with time. At the hardware trigger stage, events containing Λ_c^+ or D^0 candidates are required to match the minimum bias (MB) trigger corresponding to a requirement of at least four SPD hits or a high-p_T muon ($p_\mathrm{T} > 10$ GeV/c) or a minimal energy deposit in HCAL ($E_\mathrm{T} > 15$ GeV/c). The events are required to have at least 15 VELO tracks in the backward direction and the number of clusters (Nc) in the VELO should be at least 1000; these requirements suppress contamination from both the Pb-gas[2] and ultra-peripheral collisions. The latter are defined as electromagnetic nucleus-nucleus interactions where the impact parameter (b) is greater than the sum of the nuclei radii. Finally, events are rejected if $N_c \geq 10000$, due to hardware limitations.

The Λ_c^+ (D^0) candidates are reconstructed via the decay channel $\Lambda_c^+ \rightarrow pK^+\pi^-$ ($D^0 \rightarrow K^-\pi^+$), with a selection on transverse momentum $2 < p_\mathrm{T} < 8$ GeV/c and rapidity $2 < y < 4.5$. Offline selections are applied to the candidates following the same strategy as in pPb collisions [33] to ensure a high signal significance and improve the purity of the D^0 and Λ_c^+ candidates. Pion, kaon, and proton tracks should match tracking and particle identification (PID) quality requirements. The Λ_c^+ (D^0) decay products are required to

---

[2]Simultaneously to PbPb collisions, Neon gas was injected in the beam pipe near the interaction point, using the LHCb fixed-target SMOG system [32].

have $p_T > 400\,\text{MeV}/c$ ($p_T > 500\,\text{MeV}/c$) and $2 < y < 4.5$. The charm hadron lifetime is required to be less than 0.3 ps to reduce the fraction of non-prompt contribution coming from b-hadron decay. The cosine of the direction angle between the candidate's momentum and the vector between the PV and the candidate's decay vertex, is required to be larger than 0.9998. In addition, a fiducial cut around the beams' collision point is applied based on the PV of the Λ_c^+ and D^0 candidates.

Simulated PbPb collisions at $\sqrt{s_{NN}} = 5.02\,\text{TeV}$ with full event reconstruction are used to evaluate efficiencies. The Λ_c^+ and D^0 candidates are generated with PYTHIA 8 [34] and embedded into minimum bias PbPb collisions from the EPOS event generator [35] tuned with LHC data [36]. Decays of hadronic particles are described by EvtGen [37], in which final-state radiation is generated using PHOTOS [38]. The interaction of the generated particles with the detector, and its response, are implemented using the Geant4 toolkit [39,40] as described in Ref. [41].

3 Analysis overview

The $R_{\Lambda_c^+/D^0}$ ratio is obtained through the ratio of corrected yields as:

$$R_{\Lambda_c^+/D^0}(p_T, y \text{ or } \langle N_{\text{part}} \rangle) = \frac{\mathcal{B}^{D^0 \to K^- \pi^+}}{\mathcal{B}^{\Lambda_c^+ \to pK^+\pi^-}} \frac{Y^{\Lambda_c^+}(p_T, y \text{ or } \langle N_{\text{part}} \rangle)}{Y^{D^0}(p_T, y \text{ or } \langle N_{\text{part}} \rangle)}, \tag{1}$$

where $\mathcal{B}^{D^0} = (3.950 \pm 0.031)\%$ ($\mathcal{B}^{\Lambda_c^+} = (6.28 \pm 0.32)\%$) is the branching fraction for the D^0 (Λ_c^+) decay channel [42], respectively; p_T and y are the transverse momentum and rapidity of the D^0 (Λ_c^+) candidate; $\langle N_{\text{part}} \rangle$ is the mean number of nucleons participating in the collision; Y^{D^0} ($Y^{\Lambda_c^+}$) is the D^0 (Λ_c^+) corrected yield defined as

$$Y^{D^0, \Lambda_c^+}(p_T, y \text{ or } \langle N_{\text{part}} \rangle) = \frac{N^{D^0, \Lambda_c^+}(p_T, y \text{ or } \langle N_{\text{part}} \rangle) \cdot f_{\text{prompt}}^{D^0, \Lambda_c^+}(p_T, y \text{ or } \langle N_{\text{part}} \rangle)}{\epsilon_{\text{tot}}^{D^0, \Lambda_c^+}(p_T, y \text{ or } \langle N_{\text{part}} \rangle)}. \tag{2}$$

In Eq. 2, N^{D^0, Λ_c^+} is the inclusive number of particles measured in the PbPb dataset, and f^{D^0, Λ_c^+} is the fraction of particles produced promptly in PbPb collisions, while ϵ_{tot} is defined as the total efficiency (see Sec. 3.3). Finally, $\langle N_{\text{part}} \rangle$ is defined as the mean number of nucleons participating in the collision. A brief description of the method used to evaluate this quantity is given in Sec. 3.1.

3.1 Centrality determination

In heavy-ion collisions, centrality classes are defined as percentiles of the total inelastic hadronic PbPb cross-section and are proportional to the impact parameter b of the collision: the more central (peripheral) the collision, the smaller (greater) the b value. Likewise, $\langle N_{\text{part}} \rangle$ increases with centrality. The Glauber Monte Carlo (GMC) model [43] is used to estimate all these geometrical quantities from recorded data. A detailed description of the centrality estimation in the LHCb experiment can be found in Ref. [44]. The method is based on a binned fit of the total energy deposit in ECAL with the GMC model in MB data, collected with the same trigger conditions as that of the signal sample. Once the fit

Table 1: values of $\langle N_{part} \rangle$ in N_c intervals, with σ_{part} indicating the total systematic uncertainty of $\langle N_{part} \rangle$.

N_c interval	$\langle N_{part} \rangle$	σ_{part}
$1000 - 10000$	15.8	10.0
$1000 - 3000$	6.5	2.5
$3000 - 5500$	12.4	4.4
$5500 - 10000$	26.6	7.5

is performed, a centrality table is produced, mapping the total ECAL energy deposit and $\langle N_{part} \rangle$.

While the recorded data sample used to fit the GMC model covers the full centrality range, data used to compute $R_{\Lambda_c^+/D^0}$ are limited to $N_c < 10^4$ and centrality at about 65%. A one-to-one correspondence between ECAL and the geometrical quantity is performed on an event-by-event basis using the GMC model. Data are divided into three intervals in N_c (1000–3000, 3000–5500 and 5500–10000), based on the statistics available from the signal extraction. For each interval, other quantities (*e.g.* $\langle N_{part} \rangle$) are derived. A lower cut on N_c and on the total deposited ECAL energy to be above 310 MeV are applied to exclude the centrality range where most of the electromagnetic contamination occurs, which could bias the data. Results are given in Table 1. Three sources of systematic uncertainty associated with $\langle N_{part} \rangle$ of each interval are considered: (i) the reference hadronic cross-section parameter; (ii) the fit uncertainty; (iii) the bin size uncertainty. These uncertainties are summed in quadrature to compute the total systematic uncertainty presented in Table 1.

3.2   Signal extraction

The signal extraction is performed after the selection criteria listed in Sec. 2 are applied. Figure 1 shows the (top) $K^-\pi^+$ and (bottom) $pK^-\pi^+$ invariant-mass spectra for the selected D^0 and Λ_c^+ candidates, respectively. The data are fitted using unbinned maximum-likelihood fits combining a Crystal Ball (CB) function [45] for the signal, and a first-order polynomial function for the background. While the CB function is chosen as it models the radiative tail of the invariant mass peak, the first-order polynomial function is chosen empirically to describe the observed background. The mean and width of the CB function are left free, while other parameters are fixed with those from simulation. An alternative used to assess systematic uncertainty for the background description is to multiply the first-order polynomial by an exponential function. The total number of fitted D^0 (Λ_c^+) signal yield is 46000 (600) events.

To discriminate prompt D^0 (Λ_c^+) from those from a b-hadron decay, the background contribution is first subtracted from the datasets using the sPlot technique [46]. A fit to the $\log(\chi_{IP}^2)$ distribution is performed to discriminate the prompt from non-prompt contributions. The χ_{IP}^2 is defined as the difference in the vertex-fit χ^2 of a given PV reconstructed with and without the candidate under consideration. An example of such fit is given in Fig. 2, where the $\log(\chi_{IP}^2)$ distributions are fitted with a CB (Gaussian) function for the prompt (non-prompt) component.
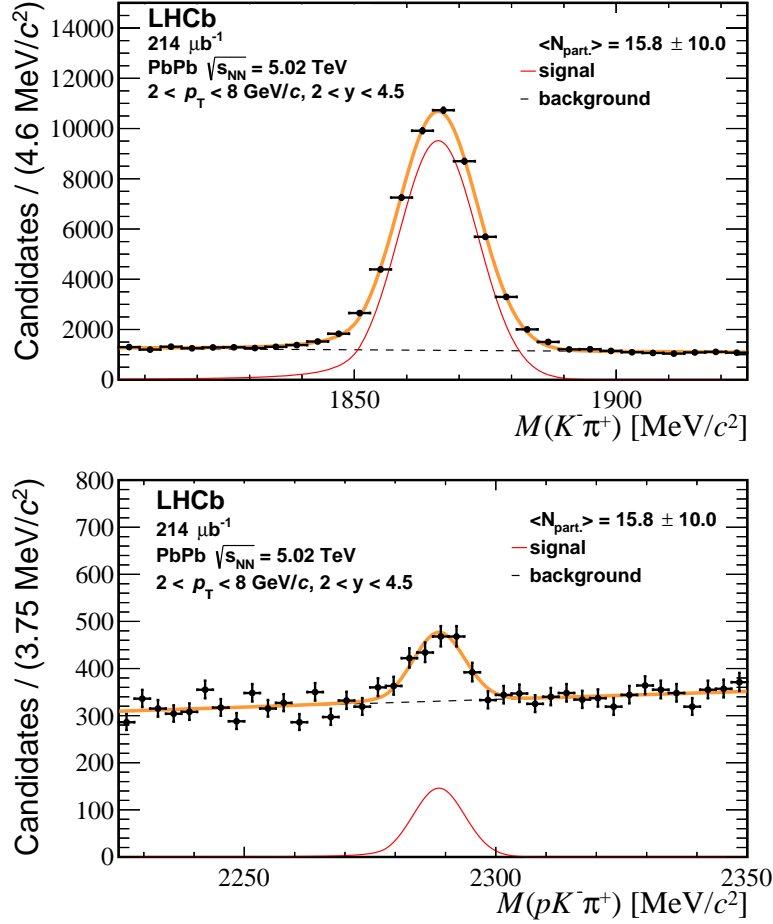
Figure 1: Invariant-mass spectra of (top) $K^-\pi^+$ and (bottom) $pK^-\pi^+$ final states. The data are overlaid with the results of the fit.

3.3 Efficiency estimation

The total efficiency (ϵ_{tot}) is factorized as

$$\epsilon_{\text{tot}}^{D^0, \Lambda_c^+}(p_{\text{T}}, y \text{ or } N_c) = \epsilon_{\text{acc}}^{D^0, \Lambda_c^+}(p_{\text{T}}, y) \times \epsilon_{\text{rec\&sel}}^{D^0, \Lambda_c^+}(p_{\text{T}}, y \text{ or } N_c) \times \epsilon_{\text{PID}}^{D^0, \Lambda_c^+}(p_{\text{T}}, y \text{ or } N_c), \quad (3)$$

where ϵ_{acc} is the acceptance efficiency; $\epsilon_{\text{rec\&sel}}$ is the reconstruction and selection efficiency; ϵ_{PID} is the PID selection efficiency; (N_c, p_{T}, y) indicate given ranges in N_c, p_{T} and rapidity.

The acceptance efficiency ϵ_{acc}, for both Λ_c^+ and D^0 hadrons, is defined as

$$\epsilon_{\text{acc}}^{D^0, \Lambda_c^+}(p_{\text{T}}, y) = \frac{N_{\text{cand}}^{2<y<4.5}}{N_{\text{cand}}^{\text{fid}}}, \quad (4)$$

where $N_{\text{cand}}^{\text{fid}}$ are simulated D^0 or Λ_c^+ yields within the fiducial acceptance and $N_{\text{cand}}^{2<y<4.5}$ indicate the number of the candidates with their decay products' rapidity within $2 < y < 4.5$. The fiducial acceptance is defined as $2 < y < 4.5$ and $2 < p_{\text{T}} < 8\,\text{GeV}/c$. This efficiency is directly computed from simulation based on PYTHIA 8.

The reconstruction and selection efficiency $\epsilon_{\text{rec\&sel}}$, for both Λ_c^+ and D^0 particles, is defined as:
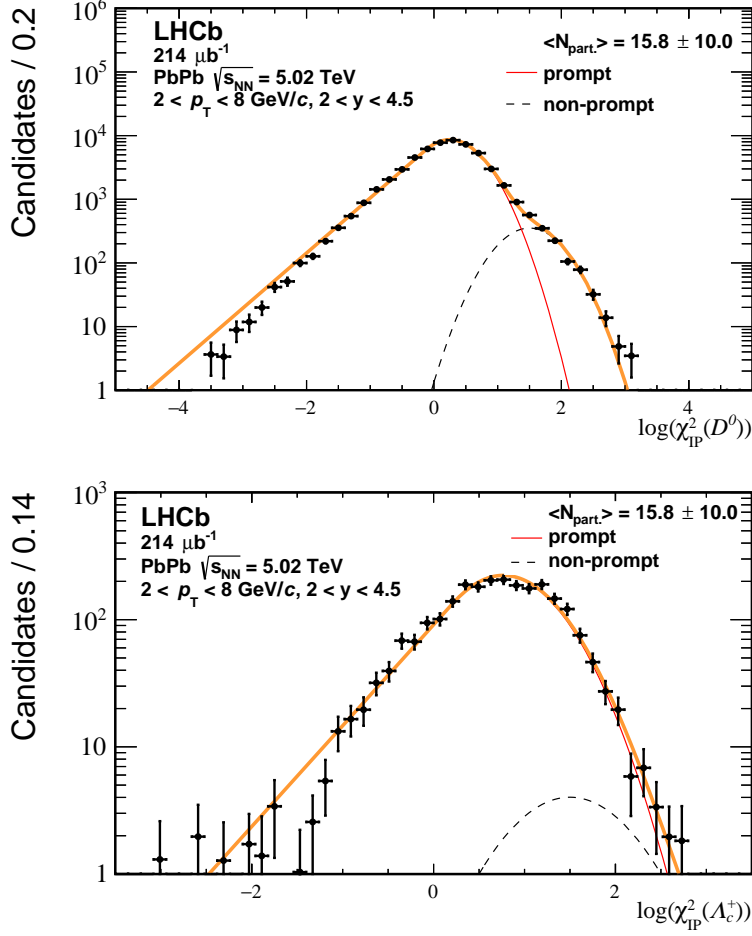
Figure 2: Distributions of $\chi^2_{\rm IP}$ of the D^0 (top) and Λ_c^+ (bottom) after background substraction. The data are overlaid with the results of the fit.

$$\epsilon^{D^0,\Lambda_c^+}_{\rm rec\&sel}(p_{\rm T}, y \text{ or } {\rm N_c}) = \frac{{\rm N}^{\rm rec.\&sel.}_{\rm cand}}{{\rm N}^{2<y<4.5}_{\rm cand}}, \tag{5}$$

where $N^{\rm rec.\&sel.}_{\rm cand}$ are reconstructed D^0 and Λ_c^+ candidates passing the selection criteria within the simulation samples. Several sources of bias are considered for $\epsilon_{\rm rec\&sel}$. The first source is the tracking algorithm efficiency, defined as the efficiency to reconstruct a track. Rather than directly measuring the tracking efficiency, the ratio of the efficiency between data and simulation is estimated using two D^0 calibration channels ($D^0 \to K^-\pi^+$ and $D^0 \to K^-\pi^+\pi^-\pi^+$). Their yields are evaluated in PbPb data and simulation and the difference of their ratio from unity is encoded in a factor k. Results are given in Table 2. Other sources of systematic uncertainty are the *ab-initio* assumptions on the $p_{\rm T}$, y and N_c distributions, and correlation effects between these variables not accounted for with the embedding technique. To account for all these effects, an iterative method based on data is employed. In the first step, the raw (i.e not corrected for inefficiency) $p_{\rm T}$, rapidity, and N_c distributions are extracted from the data based on the signal extraction defined in Sec. 3.2. In the second step, these distributions are corrected using the data-to-simulation tracking efficiency (k factor) and the PID efficiency ($\epsilon_{\rm PID}$) computed with

Table 2: Value of the k factor in intervals of N_c. The uncertainties are obtained from the statistical uncertainties of the different D^0 calibration samples in data and MC summed in quadrature.

N_c interval	$k(N_c)$
1000 – 4000	0.97±0.03
4000 – 5500	0.93±0.04
5500 – 10000	0.91±0.05

the raw kinematic distributions reconstructed in the simulation. In the third step, the reconstructed distributions from the simulation are weighted using several iterations until they match the data as a function of p_T, y, and N_c simultaneously. Finally, $\epsilon_{\text{rec\&sel}}$ is computed in step four. Steps two to four are repeated until $\epsilon_{\text{rec\&sel}}$ converges to a final value, which is the case after three iterations.

The PID efficiency ϵ_{PID} is computed using the weighted simulation samples. The methodology is similar to that used for pp collisions [47], and is based on a tag-and-probe technique. In this approach, the ϵ_{PID} for a given probe particle $\epsilon_{\text{PID}}^{\text{part}}$ (e.g. pion) is computed from a reference sample (e.g. $D^0 \to K^-\pi^+$) where a tight selection cut on the tag particle (i.e. the kaon) is applied, while no PID selection is applied to the probe particle. In the next step, the sPlot technique [46] is used to remove the background with the invariant mass as a discriminating variable. Finally, the PID efficiency of the probe is computed as the fraction of candidates (i.e. D^0) fulfilling given PID requirement.

Kaon and pion PID efficiencies are computed using the PbPb D^0 sample, while the proton efficiency is computed from $\Lambda \to \pi^- p$ decays in PbPb data. Two-dimensional maps are then computed for each particle (i.e kaon, pion, proton) as a function of p and y, for different ranges in N_c. Finally, these maps are used to compute hadron PID efficiency for D^0 and Λ_c^+ candidates as

$$\epsilon_{\text{PID}}^{D^0, \Lambda_c^+}(p_T, y \text{ or } N_c) = \frac{\prod_{\text{part}}^{\text{candidate}} \epsilon_{\text{PID}}^{\text{part}}(p, y, N_c)}{N_{\text{cand}}^{\text{rec.\&sel.}}}, \qquad (6)$$

where $\epsilon_{\text{PID}}^{\text{part}}(p, y, N_c)$ is the single-particle efficiency.

4   Systematic uncertainties

Several sources of systematic uncertainty on $R_{\Lambda_c^+/D^0}$ are considered. For the signal extraction, three parametrizations of the CB functions with different values of α are combined with the two background shapes. The systematic uncertainties are taken as the RMS of the results of all the fits for a given bin, considered as uncorrelated between the kinematic intervals. A similar strategy is employed for the prompt fraction estimation, where the Gaussian function is replaced by a Bukin function [48].

Four sources of systematic uncertainty are considered for the iterative method used to compute $\epsilon_{\text{rec\&sel}}$ and ϵ_{PID}: (i) the uncertainty on the k factor; (ii) the choice of the binning used for the reference raw data distribution; (iii) the sensitivity to the initial reference data distribution; (iv) the uncertainty on the PID maps. For each source, $\epsilon_{\text{rec\&sel}}$ and ϵ_{PID} are computed, and the RMS of all the variations are taken as the systematic

uncertainties. For the first source, new results have been obtained on $R_{\Lambda_c^+/D^0}$ using 20 values of k, varied within uncertainties. The systematic uncertainty associated with the choice of the binning scheme is evaluated by using a finer scheme than the nominal one. The sensitivity to the initial reference distributions is tested by evaluating them using an sPlot technique instead of a fit of invariant-mass spectra. Finally, the uncertainty linked to the PID maps is evaluated using a smearing technique to compute 20 PID maps where an efficiency in each bin is randomly varied within its statistical uncertainty.

All the systematic uncertainties are summarized in Table 3. Each uncertainty category is treated as uncorrelated and is added in quadrature. Systematic uncertainty arising from the $\mathcal{B}$ ratio of $D^0 \to K^-\pi^+$ and $\Lambda_c^+ \to pK^+\pi^-$ decays, entering Eq.1, is also included in Table 3. This contribution is fully correlated between different kinematic variable intervals.

Table 3: Summary of the ranges of systematic uncertainties for the considered intervals of N_c, p_{T} and y for the $R_{\Lambda_c^+/D^0}$ ratio given in percentage.

Source	N_c	p_{T} (GeV/c)	y
ϵ_{tot} (stat.)	5.1–7.1	4.1–5.1	4.1–7.1
Invariant-mass fit	1–5	1–5	1–5
f_{prompt}	1.8–8.1	1.4–10.2	3.4–4.6
ϵ_{acc}	<1	<1	<1
k factor	1.8–3.8	1.6–2.1	1.6–1.8
Iterative procedure	7–9	4–11	4–8
Total	9–12	8–14	8–10
Ratio of branching fractions	5.16	5.16	5.16

5 Results

Results for the $R_{\Lambda_c^+/D^0}$ production ratio are given in Table 4. The N_c variable is replaced by $\langle N_{part} \rangle$ as shown in Table 1. As can be seen in Fig. 3, $R_{\Lambda_c^+/D^0}$ shows no dependence on $\langle N_{part} \rangle$, within uncertainties, with a mean value $\langle R_{\Lambda_c^+/D^0} \rangle \sim 0.27$. In Fig. 4, the p_T and y dependent $R_{\Lambda_c^+/D^0}$ results are compared to those from pPb data at $\sqrt{s_{NN}} = 5.02 \, \text{TeV}$ [22], showing a good agreement between the measurements. This observation is consistent with the fact that the two samples have relatively close center-of-mass energy, and similar $\langle N_{part} \rangle$ values. The same measurements of $R_{\Lambda_c^+/D^0}$ versus p_T and y are compared to theoretical predictions in Fig. 5. Both dependencies are compared to predictions from PYTHIA 8 [15] in pp collisions at $\sqrt{s} = 5.02$ TeV. For these predictions, a special tuning is used to increase the Λ_c^+ coalescence from charm production at the expense of D mesons. In addition, the CR mechanism is also allowed. A good description of the p_T trend is found between theory and data for $p_T > 5 \, \text{GeV}/c$, while tensions are observed at low p_T. The constant trend versus rapidity is reproduced by theory predictions within three standard deviations, except for the most forward region likely due to a fluctuation in the data. The p_T dependence is also compared to predictions from the SHM [20] for which an augmented set of excited charm-baryon states decaying into Λ_c^+ is added to the fragmentation mechanism. According to this model, these additional states could explain the large $R_{\Lambda_c^+/D^0}$ observed by the ALICE experiment. These predictions are systematically higher than the LHCb data versus p_T.

Table 4: Results for the prompt $R_{\Lambda_c^+/D^0}$ production ratio, where the first uncertainties are statistical and the second systematic. A fully correlated systematic uncertainty of 5.16%, due to the limited knowledge of the external branching fractions, affects all the intervals.

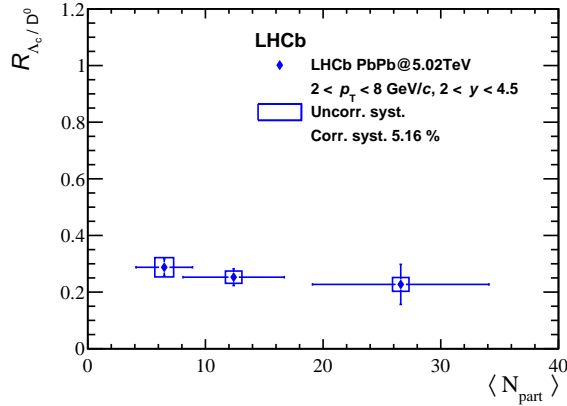| p_T (GeV/c)	$R_{\Lambda_c^+/D^0}$
$2-3$	$0.188 \pm 0.095 \pm 0.025$
$3-4$	$0.389 \pm 0.072 \pm 0.029$
$4-5$	$0.349 \pm 0.052 \pm 0.040$
$5-6$	$0.272 \pm 0.049 \pm 0.036$
$6-8$	$0.235 \pm 0.035 \pm 0.032$
y	$R_{\Lambda_c^+/D^0}$
$2.0-2.5$	$0.288 \pm 0.044 \pm 0.029$
$2.5-3.0$	$0.292 \pm 0.048 \pm 0.028$
$3.0-3.5$	$0.246 \pm 0.056 \pm 0.020$
$3.5-4.5$	$0.120 \pm 0.067 \pm 0.011$
$\langle N_{part} \rangle \pm \sigma_{part}$	$R_{\Lambda_c^+/D^0}$
6.5 ± 2.5	$0.288 \pm 0.029 \pm 0.034$
12.4 ± 4.4	$0.253 \pm 0.029 \pm 0.022$
26.6 ± 7.5	$0.227 \pm 0.071 \pm 0.024$

Figure 3: Prompt $R_{\Lambda_c^+/D^0}$ production ratios as a function of $\langle N_{part} \rangle$. The error bars along the y-axis (x-axis) represent the statistical uncertainties (RMS of the $\langle N_{part} \rangle$ value), the boxes around the points the uncorrelated systematic uncertainties.
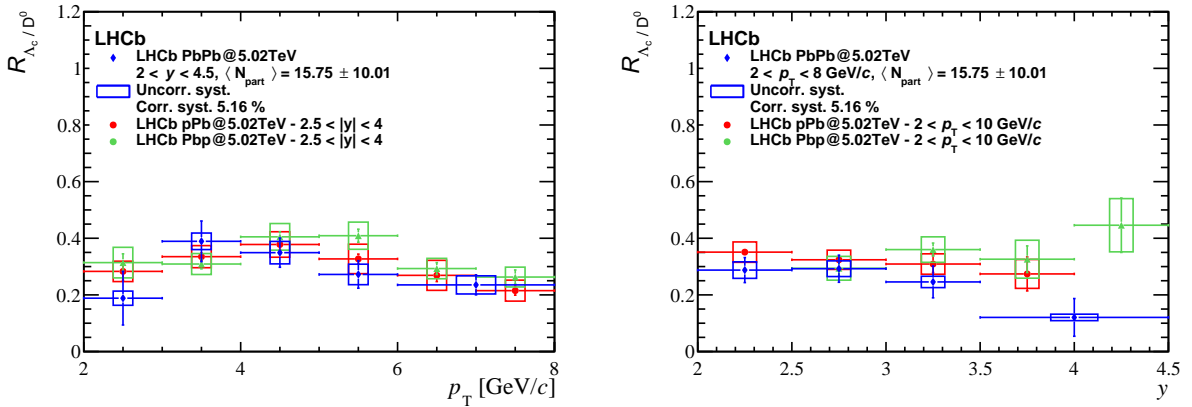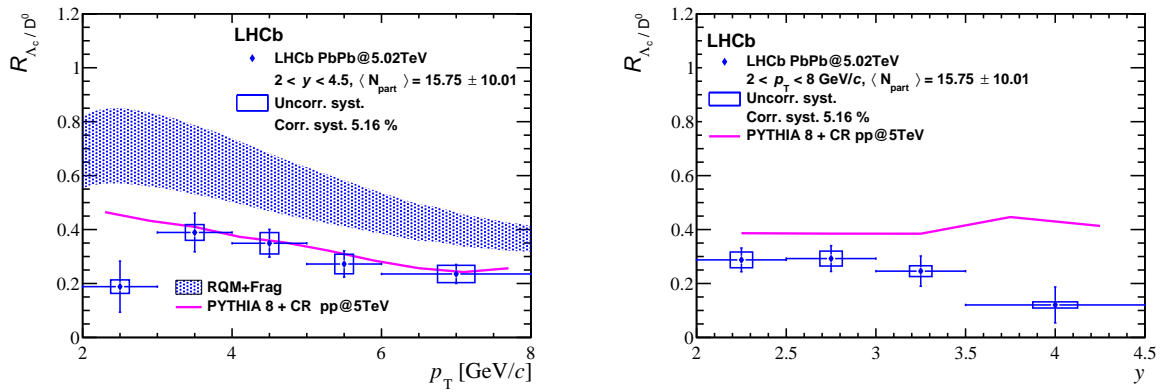

Figure 4: Prompt $R_{\Lambda_c^+/D^0}$ production ratios as a function of (left) p_T and (right) rapidity. The error bars represent the statistical uncertainties, the boxes around the points the uncorrelated systematic uncertainties. Results are compared to the same measurement in pPb and Pbp collisions at $\sqrt{s_{NN}} = 5.02$ TeV by the LHCb experiment [33].

10

Figure 5: Prompt $R_{\Lambda_c^+/D^0}$ production ratios as a function of (left) p_{T} and (right) rapidity. The error bars represent the statistical uncertainties, the boxes around the points the uncorrelated systematic uncertainties. Results are compared to PYTHIA 8 [15] in pp collisions at $\sqrt{s} = 13$ TeV (magenta band) and predictions from a Statical Hadronization Model [20] (blue band).

6 Conclusions

This paper reports the first measurements of the $R_{\Lambda_c^+/D^0}$ production cross-section ratio in peripheral PbPb collisions at $\sqrt{s_{\mathrm{NN}}} = 5.02$ TeV by the LHCb experiment. The $R_{\Lambda_c^+/D^0}$ shows no significant dependence on either rapidity or $\langle \mathrm{N_{part}} \rangle$ within uncertainties, and has a mean value of $\langle R_{\Lambda_c^+/D^0} \rangle \sim 0.27$. However, the ratio tends to decrease at lower p_{T}. More data are needed to confirm the results. Results are consistent with previous LHCb measurements in pPb collisions at $\sqrt{s_{\mathrm{NN}}} = 5.02$ TeV [33]. Compared to theory predictions, the results are compatible within one standard deviation with the PYTHIA 8 predictions in pp collisions at $\sqrt{s} = 5.02$ TeV, including the CR mechanism, except at low p_{T}. In contrast, a systematic discrepancy versus p_{T} is observed with the SHM model predictions. These new experimental results point toward a strong dependence of $R_{\Lambda_c^+/D^0}$ with rapidity, which helps to constrain theory predictions in this particular phase-space region.

References

[1] P. Braun-Munzinger, V. Koch, T. Schäfer, and J. Stachel, *Properties of hot and dense matter from relativistic heavy ion collisions*, Phys. Rept. **621** (2016) 76, arXiv:1510.00442.

[2] HotQCD collaboration, A. Bazavov *et al.*, *Equation of state in (2+1)-flavor QCD*, Phys. Rev. **D90** (2014) 094503, arXiv:1407.6387.

[3] P. B. Gossiaux, *Open heavy flavours in nuclear collisions: Theory overview*, Nucl. Phys. **A982** (2019) 113, arXiv:1901.01606.

[4] A. Andronic *et al.*, *Heavy-flavour and quarkonium production in the LHC era: from proton–proton to heavy-ion collisions*, Eur. Phys. J. **C76** (2016) 107, arXiv:1506.03981.

[5] F. Prino and R. Rapp, *Open heavy flavor in QCD matter and in nuclear collisions*, J. Phys. **G43** (2016) 093002, arXiv:1603.00529.

[6] CLEO collaboration, M. Artuso *et al.*, *Charm meson spectra in e^+e^- annihilation at 10.5 GeV center of mass energy*, Phys. Rev **D70** (2004) 112001, arXiv:hep-ex/0402040.

[7] Belle collaboration, R. Seuster *et al.*, *Charm hadrons from fragmentation and B decays in e^+e^- annihilation at $\sqrt{s}$ = 10.6 GeV*, Phys. Rev. **D73** (2006) 032002, arXiv:hep-ex/0506068.

[8] BaBar collaboration, B. Aubert *et al.*, *Measurement of D_s^+ and D_s^{*+} production in B meson decays and from continuum e^+e^- annihilation at $\sqrt{s}$ = 10.6 GeV*, Phys. Rev. **D65** (2002) 091104, arXiv:hep-ex/0201041.

[9] LHCb collaboration, R. Aaij *et al.*, *Prompt charm production in pp collisions at $\sqrt{s}$ = 7 TeV*, Nucl. Phys. **B871** (2013) 1, arXiv:1302.2864.

[10] LHCb collaboration, R. Aaij *et al.*, *Measurements of prompt charm production cross-sections in pp collisions at $\sqrt{s}$ = 13 TeV*, JHEP **03** (2016) 159, Erratum ibid. **09** (2016) 013, Erratum ibid. **05** (2017) 074, arXiv:1510.01707.

[11] LHCb collaboration, R. Aaij *et al.*, *Measurements of prompt charm production cross-sections in pp collisions at $\sqrt{s}$ = 5 TeV*, JHEP **06** (2017) 147, arXiv:1610.02230.

[12] ALICE collaboration, S. Acharya *et al.*, *Λ_c^+ production in pp collisions at $\sqrt{s}$ = 7 TeV and in p-Pb collisions at $\sqrt{s_{NN}}$ = 5.02 TeV*, JHEP **04** (2018) 108, arXiv:1712.09581.

[13] ALICE collaboration, S. Acharya *et al.*, *Λ_c^+ production in Pb-Pb collisions at $\sqrt{s_{NN}}$ = 5.02 TeV*, Phys. Lett. **B793** (2019) 212, arXiv:1809.10922.

[14] ALICE collaboration, S. Acharya *et al.*, *Λ_c^+ production in pp and in p-Pb collisions at $\sqrt{s_{NN}}$ = 5.02 TeV*, Phys. Rev. **C104** (2021) 054905, arXiv:2011.06079.

[15] J. R. Christiansen and P. Z. Skands, *String formation beyond leading colour*, JHEP **08** (2015) 003, arXiv:1505.01681.

[16] S. Plumari *et al.*, *Charmed hadrons from coalescence plus fragmentation in relativistic nucleus-nucleus collisions at RHIC and LHC*, Eur. Phys. J. **C78** (2018) 348, arXiv:1712.00730.

[17] CMS collaboration, A. M. Sirunyan *et al.*, *Production of Λ_c^+ baryons in proton-proton and lead-lead collisions at $\sqrt{s_{\mathrm{NN}}} = 5.02$ TeV*, Phys. Lett. **B803** (2020) 135328, arXiv:1906.03322.

[18] STAR collaboration, J. Adam *et al.*, *First measurement of Λ_c^+ baryon production in Au+Au collisions at $\sqrt{s_{\mathrm{NN}}} = 200$ GeV*, Phys. Rev. Lett. **124** (2020) 172301, arXiv:1910.14628.

[19] Y. Oh, C. M. Ko, S. H. Lee, and S. Yasui, *Heavy baryon/meson ratios in relativistic heavy ion collisions*, Phys. Rev. **C79** (2009) 044905, arXiv:0901.1382.

[20] M. He and R. Rapp, *Hadronization and charm-hadron ratios in heavy-ion collisions*, Phys. Rev. Lett. **124** (2020) 042301, arXiv:1905.09216.

[21] M. He and R. Rapp, *Charm-baryon production in proton-proton collisions*, Phys. Lett. **B795** (2019) 117, arXiv:1902.08889.

[22] LHCb collaboration, R. Aaij *et al.*, *Prompt Λ_c^+ production in pPb collisions at $\sqrt{s_{NN}} = 5.02$ TeV*, JHEP **02** (2019) 102, arXiv:1809.01404.

[23] K. J. Eskola, H. Paukkunen, and C. A. Salgado, *EPS09: A new generation of NLO and LO nuclear parton distribution functions*, JHEP **04** (2009) 065, arXiv:0902.4154.

[24] K. Kovarik *et al.*, *nCTEQ15 - Global analysis of nuclear parton distributions with uncertainties in the CTEQ framework*, Phys. Rev. **D93** (2016) 085037, arXiv:1509.00792.

[25] LHCb collaboration, A. A. Alves Jr. *et al.*, *The LHCb detector at the LHC*, JINST **3** (2008) S08005.

[26] LHCb collaboration, R. Aaij *et al.*, *LHCb detector performance*, Int. J. Mod. Phys. **A30** (2015) 1530022, arXiv:1412.6352.

[27] R. Aaij *et al.*, *Performance of the LHCb Vertex Locator*, JINST **9** (2014) P09007, arXiv:1405.7808.

[28] P. d'Argent *et al.*, *Improved performance of the LHCb Outer Tracker in LHC Run 2*, JINST **12** (2017) P11016, arXiv:1708.00819.

[29] M. Adinolfi *et al.*, *Performance of the LHCb RICH detector at the LHC*, Eur. Phys. J. **C73** (2013) 2431, arXiv:1211.6759.

[30] A. A. Alves Jr. *et al.*, *Performance of the LHCb muon system*, JINST **8** (2013) P02022, arXiv:1211.1346.

[31] R. Aaij *et al.*, *The LHCb trigger and its performance in 2011*, JINST **8** (2013) P04022, arXiv:1211.3055.

[32] LHCb collaboration, R. Aaij *et al.*, *Precision luminosity measurements at LHCb*, JINST **9** (2014) P12005, `arXiv:1410.0149`.

[33] LHCb collaboration, R. Aaij *et al.*, *Prompt Λ_c^+ production in pPb collisions at $\sqrt{s_{NN}} = 5.02$ TeV*, JHEP **02** (2019) 102, `arXiv:1809.01404`.

[34] T. Sjostrand, S. Mrenna, and P. Z. Skands, *A brief introduction to PYTHIA 8.1*, Comput. Phys. Commun. **178** (2008) 852, `arXiv:0710.3820`.

[35] S. Porteboeuf, T. Pierog, and K. Werner, *Producing hard processes regarding the complete event: the EPOS event generator*, 45th Rencontres de Moriond on QCD and High Energy Interactions (2010) 135, `arXiv:1006.2967`.

[36] T. Pierog *et al.*, *EPOS LHC: Test of collective hadronization with data measured at the CERN large hadron collider*, Phys. Rev. **C92** (2015) 034906, `arXiv:1306.0121`.

[37] D. J. Lange, *The EvtGen particle decay simulation package*, Nucl. Instrum. Meth. **A462** (2001) 152.

[38] P. Golonka and Z. Was, *PHOTOS Monte Carlo: A precision tool for QED corrections in Z and W decays*, Eur. Phys. J. **C45** (2006) 97, `arXiv:hep-ph/0506026`.

[39] Geant4 collaboration, S. Agostinelli *et al.*, *Geant4: A simulation toolkit*, Nucl. Instrum. Meth. **A506** (2003) 250.

[40] Geant4 collaboration, J. Allison *et al.*, *Geant4 developments and applications*, IEEE Trans. Nucl. Sci. **53** (2006) 270.

[41] M. Clemencic *et al.*, *The LHCb simulation application, Gauss: Design, evolution and experience*, J. Phys. Conf. Ser. **331** (2011) 032023.

[42] Particle Data Group, P. A. Zyla *et al.*, *Review of particle physics*, Prog. Theor. Exp. Phys. **2020** (2020) 083C01.

[43] C. Loizides, J. Nagle, and P. Steinberg, *Improved version of the PHOBOS Glauber monte carlo*, doi: 10.1016/j.softx.2015.05.001 `arXiv:1408.2549`.

[44] LHCb collaboration, R. Aaij *et al.*, *Centrality determination in heavy-ion collisions with the LHCb detector*, `arXiv:2111.01607`.

[45] T. Skwarnicki, *A study of the radiative cascade transitions between the Upsilon-prime and Upsilon resonances*, PhD thesis, Institute of Nuclear Physics, Krakow, 1986, DESY-F31-86-02.

[46] M. Pivk and F. R. Le Diberder, *sPlot: A statistical tool to unfold data distributions*, Nucl. Instrum. Meth. **A555** (2005) 356, `arXiv:physics/0402083`.

[47] L. Anderlini *et al.*, *The PIDCalib package*, LHCb-PUB-2016-021, 2016.

[48] A. D. Bukin, *Fitting function for asymmetric peaks*, `arXiv:0711.4449`.